Auxiliary-Less Precharge Strategy for Flying-Capacitor Current-Fed DAB Converters

Takashi Ohno[1]*, Hiroki Watanabe[2], Jun-ichi Itoh[2]
1 Department of Science of Technology Innovation, Nagaoka University of Technology, Niigata, Japan
2 Department of Electrical, Electronics, and Information Engineering, Niigata, Japan
*s225058@stn.nagaokaut.ac.jp

***Abstract*—This paper proposes an auxiliary-less precharging method for all capacitors, including flying capacitors, in a flying-capacitor current-fed dual active bridge converter. The converter employs a small magnetizing inductance to achieve zero-voltage switching over the entire operating range. The duty ratio is determined by a control scheme that dynamically limits the transformer peak current and the boost inductor peak current, enabling fast precharging while preventing magnetic saturation. The precharging process is divided into multiple sequences, with the duty ratio adjusted according to the operating mode. Due to parameter tolerances of passive components, deviations from simulation are observed. However, the errors are limited to 12% at 150 V. and 5% at 500 V. Experimental results confirm that the transformer and boost-inductor currents are clamped to 50 A, validating the proposed method.**

Keywords— dual active bridge converter, flying-capacitor converters, multilevel, initial charging strategy.

I. Introduction

In recent years, the spread of AI servers and cloud servers has led to the installation of megawatt-class data centers.[1][2] As a result, the power supply systems have become larger, and modular configurations that use multiple converters in parallel have been adopted in megawatt-class power supplies in order to improve efficiency and scalability. In such configurations, each module is repeatedly turned on and off according to the load to maintain the overall conversion efficiency. In addition, DC-bus voltages of 380 V and 800 V have been investigated for data-center applications. However, a DC-bus voltage of 1500 V is also a strong candidate in order to accommodate large power capacity and compatibility with renewable energy sources [3][4][5].

With the increase in voltage, multilevel circuits have been considered strong candidates[6], particularly flying-capacitor topologies, to improve circuit performance[7][8][9]. However, the voltage management of the flying capacitors is an important issue. In applications where startup and shutdown are repeated, each capacitor, including the flying capacitors, must be charged to the specified voltage within a short period in order to ensure stable system operation. Previous studies have mainly discussed precharging methods for non-isolated converters and inverters[10][11]. Most of these methods realize precharging by employing additional components such as resistors and diodes. However, these approaches increase both cost and volume.

In the isolated DC-DC converters, such as the Dual Active Bridge (DAB) converter, precharging methods for the output capacitors have also been investigated. One method operates only on the primary side, while the secondary side operates as a rectifier[12]. The duty ratio is controlled in order to avoid transformer saturation. However, as the output voltage increases, the charging current decreases, resulting in a longer charging time. Moreover, the maximum output voltage is limited to the secondary-referred input voltage. On the other hand, some studies have considered DAB operation that transfers power from the primary side to the secondary side to charge the output capacitors. However, the studies have not sufficiently considered the effect of the magnetizing inductance [13].

This paper proposes an initial charge method for the flying-capacitor current-fed DAB (FCCF-DAB) converter that achieves the precharging of all capacitors, including the flying capacitors. The FCCF-DAB converter is designed with relatively small magnetizing inductance in order to achieve zero-voltage switching (ZVS) over the entire operating range.

The main contribution of this paper is an auxiliary-less precharging strategy for the flying-capacitor current-fed DAB converter, which enables all capacitors, including the flying capacitors, to be charged without additional dedicated components. The proposed method strictly maintains both the transformer and boost-inductor currents within their designed saturation limits throughout the entire precharging sequence, achieving fast, simple, and highly reliable initialization as demonstrated by simulation and experimental results.

II. Circuit Configuration

Fig. 1 shows the circuit configuration of the FCCF-DAB converter with the precharging scheme. A precharging resistor R_{pre} for inrush current limitation is connected in parallel with the primary-voltage side relay. Also, the secondary side is connected to the 1500 V grid using a DC relay. Furthermore, these relays and the low-side precharge resistor are commonly used components, which are not additional components dedicated to precharging, and an anti-windup PI controller employed.

In this circuit configuration, the precharging operation is not performed from the secondary-voltage side. The flying capacitor and output capacitor are charged by transmitting power from the primary side. Then, the relay on the output side is turned on when the voltage of the output capacitor matches the DC grid voltage.

III. Precharging Sequences and Control Method

Fig. 2 shows the flowchart of the precharging operation. In Sequence 0, the input capacitor C_{in} and DC-bus capacitor

This work was supported by JST SPRING, Japan Grant Number JPMJSP2189.

C_{dc} are charged up to battery voltage V_{bat} through the precharging resistor. When the voltages of C_{in} and C_{dc} reach V_{bat}, the control transitions to Sequence 1. In Sequence 1, the primary-side PWM is enabled to charge the C_{dc}, the flying capacitors C_{fcc} and C_{fcd}, and the output capacitor C_{out}. The control transitions to Sequence 2 when C_{fcc} and C_{fcd} reach to 750 V, and Cdc reaches 800 V. The value of 750 V corresponds to half of V_{grid}. The value of 800 V corresponds to the command DC-bus voltage. In Sequence 2, C_{out} is charged up to the DC-grid voltage V_{grid}, which completes the precharging process.

Fig. 3 shows the control block diagram of the precharging operation in the FCCF-DAB converter. The inner loop includes a current controller that regulates the input current. The outer loop includes a voltage controller that regulates the DC-bus voltage. Each controller is implemented using an anti-windup PI controller.

A limit is imposed on the input-current command to restrict the peak current of the boost inductor. This limit may allow the input current Iin to exceed the rated value, depending on the input voltage Vin and the DC-bus voltage Vdc. The proposed method does not impose a current limit based on thermal constraints to achieve rapid precharging within a short duration. In addition, the limit before the duty command D1 is introduced in order to prevent the transformer peak current from exceeding the design value. Thus, the duty ratio is adjusted according to each capacitor voltage to prevent saturation of both the boost inductor and the transformer. The charging current is limited to the designed maximum value of the magnetic components.

A. Initial charging sequence

As mentioned in the previous section, C_{in} and C_{dc} are charged through R_{pre} in sequence 0. When a step voltage is applied from the V_{bat} side, which occurs when the N-side relay on the primary side is turned on, the maximum value of the inrush current flowing into C_{in} is determined by R_{pre} and the V_{bat}. Therefore, R_{pre} is designed based on Ohm's law in order to ensure that the maximum inrush current does not exceed the maximum current specified in the circuit design. In Sequence 0, the control transitions to the next sequence when V_{in} and V_{dc} reach V_{bat}. The control then enables the positive-side input relay.

In sequence 1, the primary-side PWM is enabled in order to charge C_{dc}, C_{fcc}, C_{fcd}, and C_{out}. In addition, the lowest switches on the secondary side, S_8 and S_{12}, are turned on continuously. As a result, C_{fcc} and C_{fcd} are connected in parallel with C_{out}, which causes the secondary-side capacitor to be charged uniformly. In Sequence 1, the control charges the flying capacitors C_{fcc} and C_{fcd} to 750 V, corresponding to half of V_{grid}, while regulating V_{dc} to its command V_{dc}^*. The charging of C_{fcc} and C_{fcd} can be stopped by turning off switch Q_8 or Q_{12}, respectively. The control transitions to Sequence 2 after the completion of the charging operation.

In sequence 2, C_{out} is charged up to V_{grid}. However, the condition that L_m is sufficiently larger than L_{dab} is not satisfied. Therefore, C_{out} cannot be charged up to V_{grid} only by switching the primary side as in Sequence 1 or Sequence 2. In addition, as V_{dc} and V_{trp} become asymptotic, the transformer current decreases, and the charging process requires a longer time.

Therefore, DAB operation is performed in order to transfer power to the secondary side by switching both the primary

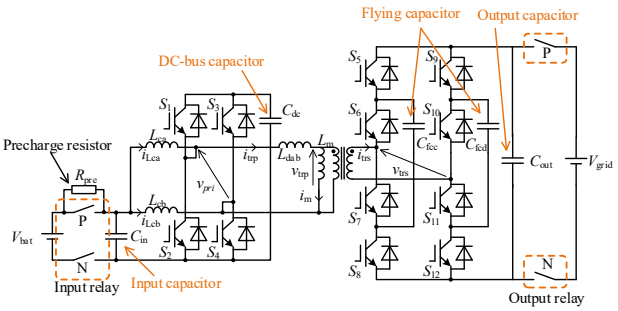

Fig. 1 Circuit configuration of the FCCF-DAB converter considering the precharging operation. The N-side input relay is turned on to charge C_{in} and C_{dc} up to V_{bat} through the precharge resistor. The P-side input relay is then turned on to start the precharging operation. The output-side relay is turned on after the completion of the precharging process.

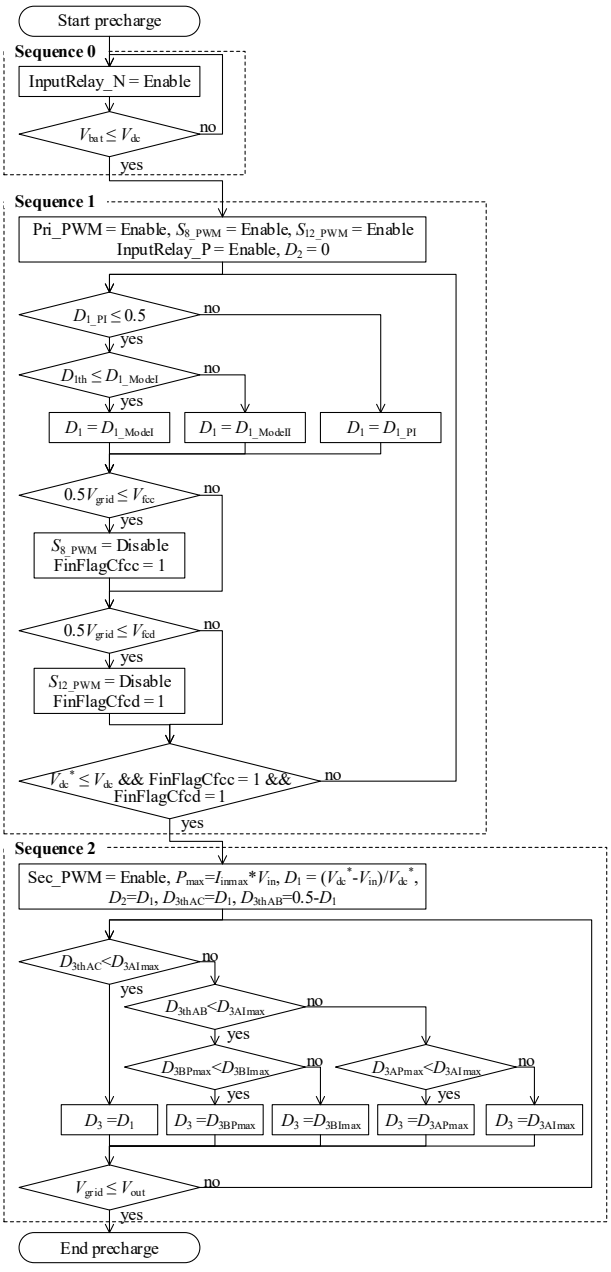

Fig. 2 Precharging flow of the FCCF-DAB converter. In Sequence 0, charging is performed through the precharge resistor. In Sequence 1, switching of the primary side completes the charging of C_{dc}, C_{fcc}, and C_{fcd}. In Sequence 2, DAB operation completes the charging of C_{out}.

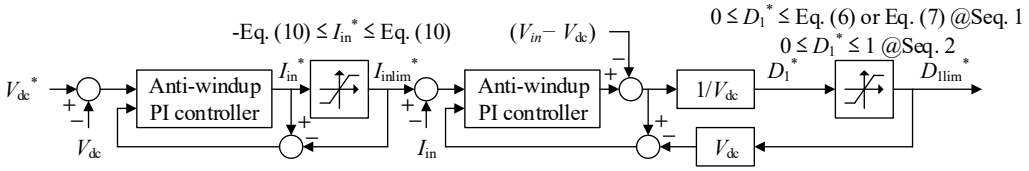

Fig. 3 Control block diagram of the precharging operation. The control structure consists of an inner input-current controller and an outer DC-bus voltage controller. The output limit of the voltage controller restricts the peak current of the boost inductor. The output limit of the current controller restricts the peak transformer current.

side and the secondary side, so that C_{out} is charged up to V_{grid}. The primary-side duty ratio is determined by the boosting ratio and is expressed as

$$D_1 = \frac{V_{dc}^* - V_{in}}{V_{dc}^*}, \tag{1}$$

where V_{dc}^* is the command value of the DC-bus voltage, which is 800 V, and V_{in} is the input capacitor voltage.

The same value as D_1 is used for the secondary-side duty D_2 in order to simplify the implementation. Sequence 2 ends after C_{out} is charged up to V_{grid}, and the precharging process is completed.

Fig. 4 shows the relationship between the three transformer current modes and the phase-shift duty in the FCCF-DAB converter. Thus, in Sequence 2, three transformer current modes must be considered to control the transformer current and the power appropriately. The current modes are classified as modes A, B, and C. These modes correspond to Mode III, Mode IV, and Mode V in [14], respectively. In mode C, the transmitted active power does not depend on the phase shift, and the phase-shift duty is set to D_1, which corresponds to the maximum-power condition. D_{3APmax} and D_{3BPmax} are derived from a conventional power equation presented in [14], where the maximum transferable power that does not cause saturation of the boost inductor is used as the power command. D_{3Aimax} and D_{3BImax} are calculated as the maximum phase shift values that do not cause transformer saturation under the given voltage conditions and duty ratios D_1 and D_2. These expressions are derived based on the theoretical current waveforms presented in [14]. These conditions define the saturation constrains of the boost inductor current and transformer current. The smaller value is selected in each phase shift duty. D_{3APmax}, D_{3BPmax}, D_{3AImax}, and D_{3BImax} are expressed as

$$D_{3APmax} = D_1 - \sqrt{D_1^2 - \frac{P_{max} f_s L_{dab}}{V_{dc} V_{trp}}}, \tag{2}$$

$$D_{3AImax} = \frac{2L_{dab} f_s I_{trp.max} + (V_{trp} - V_{dc}) D_1}{2V_{trp}}, \tag{3}$$

$$D_{3BPmax} = \frac{1}{2}\left(\frac{1}{2} - \sqrt{-\frac{1}{4} + 2D_1 - 2D_1^2 - \frac{2P_{max} L_{dab} f_s}{V_{dc} V_{trp}}}\right), \tag{4}$$

$$D_{3BImax} = \frac{2L_{DAB} f_s I_{trp.max} + (V_{dc} - V_{trp}) D_1}{2V_{dc}}, \tag{5}$$

where P_{max} is the maximum transferable power from the primary side to the secondary side, f_s is the switching frequency, L_{dab} is the sum of the external inductor and leakage inductor of the transformer, V_{trp} is the primary-side transformer voltage, V_{dc} is the DC-bus capacitor voltage, I_{trpmax} is the transformer peak current.

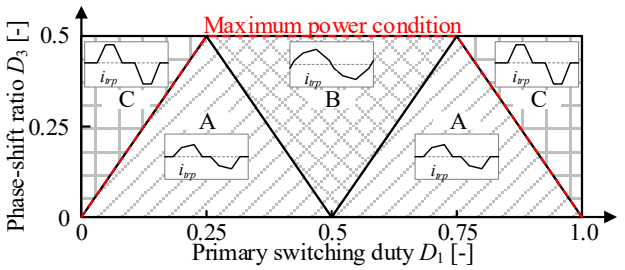

Fig. 4 Three operation regions of the FCCF-DAB converter. The operating region transitions according to the boosting ratio and the transmitted power. In mode C, the transmitted power does not increase through the phase shift between the bridges, which makes the maximum-power condition the boundary between region A and C.

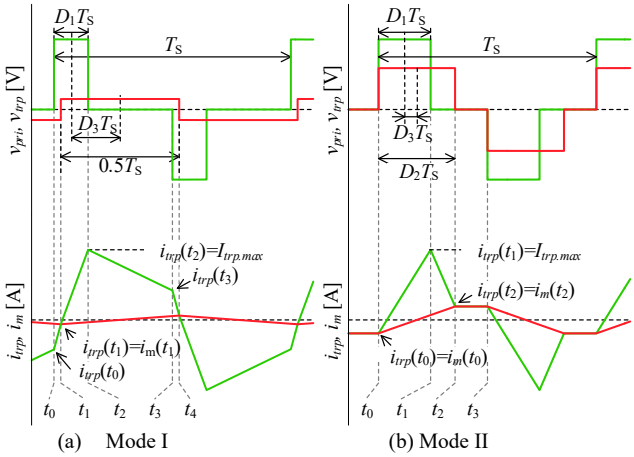

Fig. 5 Two operational waveforms during the precharging period when only the primary side is switching. The primary-side switching duty D_1 is controlled to maintain the transformer peak current up to the saturation current.

In Sequence 2, the initial charging operation completes when C_{out} reaches the grid voltage of 1500 V. The control then turns on the output-side relay.

B. Transformer current constraints

During the charging of the secondary-side capacitors, power transfer is carried out through the transformer. Therefore, the primary-duty ratio must be carefully determined in order to prevent saturation of the transformer and the external inductor. In particular, the external inductor is designed based on the saturation current value. Depending on the bridge-to-bridge voltage and the conduction angle of the current, the inductor current may exceed the design current value.

Fig. 5 shows the operating waveforms during the precharging process of Sequence 1. The converter operates in mode I when the output capacitor voltage is sufficiently low. When the output capacitor voltage is partially charged, the converter operates in mode II.

In this circuit configuration, the magnetizing inductance is designed to be relatively small in order to achieve ZVS over the entire operating range. Therefore, it is necessary to consider the magnetizing current to maintain the maximum current of the transformer. According to the definition in Fig. (5), the transformer current reaches its maximum at time t_2 in Mode I. The transformer current at time t_2 in Mode I is expressed as

$$i_{trp\_Model}(t_2)=\frac{V_{dc}-V_{trp}}{L_{dab}}(t_2-t_1)+i(t_1). \tag{6}$$

The transformer current and the magnetizing current are equal at $i_{trp.modeI}(t_1)$. The magnetizing current has a triangular waveform, and the maximum value can be calculated. The relationships are expressed as

$$i_{trp\_Model}(t_1)=-I_{m\_Model}(t_1)=-\frac{V_{trp}}{4L_m f_s}, \tag{7}$$

where the L_m is the magnetizing inductance.

The time t_1 in Mode I is derived based on the current equations in the intervals t_0-t_1, t_1-t_2, t_2-t_3, and t_3-t_4. The time t_1 is expressed as

$$t_{1\_Model}=\frac{1}{2f_s}\left(D_1-\frac{1}{2}\frac{V_{trp}}{V_{dc}}-\frac{1}{2}\frac{L_{dab}V_{trp}}{L_m V_{dc}}\right). \tag{8}$$

From (6), (7), and (8), the command value of D_1 in Mode I is expressed as

$$D_{1\_Model}=\left(2I_{trp.max}f_s+\frac{V_{trp}}{2L_m}\right)\frac{L_{dab}}{V_{dc}-V_{trp}}-\frac{V_{trp}}{2V_{dc}}\left(1+\frac{L_{dab}}{L_m}\right). \tag{9}$$

According to the definition in Fig. 5(b), the current at time t_1 becomes the maximum transformer current in Mode II. The equality between $i(t_0)$ and $-i(t_3)$ is satisfied. The transformer current at time t_0 and the current at time t_2 are expressed as

$$i_{trp\_ModeII}(t_0)=\frac{V_{trp}}{2L_{dab}}t_2-\frac{V_{dc}-V_{trp}}{2L_{dab}}\frac{D_1}{f_s}. \tag{10}$$

$$i_{ModeII}(t_2)=\frac{V_{dc}-V_{trp}}{L_{dab}}\frac{D_1}{f_s}+\frac{-V_{trp}}{L_{dab}}\left(t_2-\frac{D_1}{f_s}\right)=\frac{V_{trp}}{L_m}t_2. \tag{11}$$

The current $i_{ModeII}(t_1)$ is expressed as

$$i_{ModeII}(t_1)=\frac{V_{dc}-V_{trp}}{L_{dab}}t_2+i_{trp\_ModeII}(t_0), \tag{12}$$

From (10), (11), and (12), the relationship between the maximum transformer current $I_{trp.max}$ and D_1 is derived by solving for D_{1_ModeII}. The relationship is expressed as

$$D_{1\_ModeII}=\frac{2f_s I_{trp.max}L_{dab}(L_m+L_{dab})}{V_{dc}(2L_m+L_{dab})-2V_{trp}(L_m+L_{dab})}, \tag{13}$$

In addition, the boundary condition between mode I and mode II is expressed as

$$D_{1th}=\frac{V_{trp}}{2V_{dc}}\left(\frac{L_{dab}}{L_m}+1\right). \tag{14}$$

The calculation result obtained from (9) is compared with the boundary condition defined by (14). (9) is selected if the calculation result is larger, whereas (13) is selected if it is smaller.

The transformer current increases as the primary-duty ratio D_1 approaches 0.5. The command value of primary-duty ratio D_1^* exceeds 0.5 under the condition that the boost ratio from the input voltage V_{in} to the DC-bus voltage V_{dc} is higher than 2. The transformer current decreases when the D_1 exceeds 0.5. The PI controller charges V_{dc} to V_{dc}^* after the D_1^* exceeds 0.5.

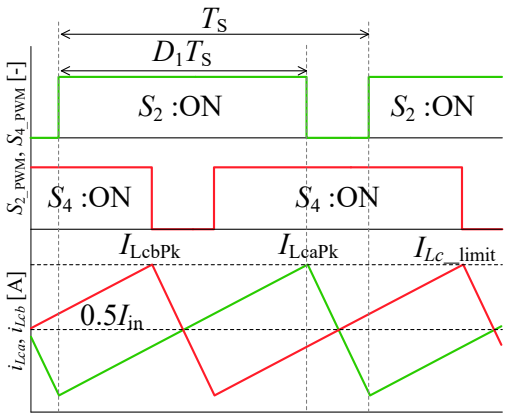

Fig. 6 Theoretical waveforms of the boost inductor current. During the precharging operation, V_{in} and V_{dc} vary dynamically. The primary-side duty ratio must be calculated to maintain an appropriate peak current and to prevent saturation of the boost inductor.

C. Boost inductor current constraints

In the initial stage of Sequence 1, the difference between the DC-bus voltage and the primary-side transformer voltage, which corresponds to the output voltage converted by the turns ratio, is extremely large. The current limit is mainly determined by the transformer peak current. During the middle and final stages of Sequence 1 and during Sequence 2, the DC-bus voltage gradually approaches the primary-side transformer voltage. The current limitation is then determined by the boost inductor peak current. This paper achieves a seamless transition from transformer current limitation to boost inductor current limitation by using a PI controller that includes an anti-windup.

Fig. 6 shows the theoretical waveform of the boost inductor current. The relationship between the average value of the boost inductor current and the peak current is expressed as [15]

$$I_{LcPk}=\frac{1}{2}\left(I_{in}+\frac{V_{in}}{L_c f_s}D_1\right), \tag{15}$$

where I_{in} is the input current, and L_c is the boost inductance.

The first term in the parentheses of (15) represents the DC-component of the boost inductor current. The second term represents the ripple component and corresponds to the variation of the inductor current over one switching period. I_{in} represents the DC on the input side. The peak value of the boost inductor current can be effectively limited by applying an appropriate limit value to the current command. The specific limit value of the input current command is expressed by

$$I_{inmax}=2I_{LcPk}-\frac{V_{in}}{L_c f_s}D_1. \tag{16}$$

The input current limitation based on (16) can allow a current that exceeds the rated current. The proposed method assumes a short-duration operation corresponding to the precharging process. The precharging process is completed within a duration that is sufficiently shorter than the thermal time constants of the switching devices and the winding of the

magnetic components. The current limitation is determined based only on the saturation flux density in order to simplify the design. The determination of a specific current limit based on thermal design remains a subject for future work.

IV. Simulation Results

Table I shows the circuit parameters used for the simulation and the experiments. The maximum current of the magnetic components, boost inductor L_c and L_{dab}, is 50 A for both.

TABLE I. Circuit Parameters

Element	Symbol	Value
Rated power	P_{rated}	20 kW
Boost inductor peak current	I_{LcPk}	50 A
Max. primary side transformer current	$I_{trp.max}$	50 A
Battery voltage	V_{bat}	150 – 500 V
DC-bus voltage command	V_{dc}^*	800 V
Flying capacitor voltage command	V_{fcc}^*, V_{fcd}^*	750 V
DC-grid voltage	V_{grid}	1500 V
Switching frequency	f_s	10 kHz
Boost inductor	L_{ca}, L_{cb}	333 µH
External inductor + leakage inductor	L_{dab}	108 µH
Magnetizing inductor	L_m	711 µH
Input capacitor	C_{in}	1650 µF
DC-bus capacitor	C_{dc}	1950 µF
Flying capacitor	C_{fcc}, C_{fcd}	227 µF
Output capacitor	C_{out}	1300 µF

Fig. 7 shows the simulation waveforms of the FCCF-DAB converter from Sequence 0 to the completion of the precharging process. The primary-side duty command is applied in a ramp shape in order to prevent inrush current at the beginning of switching in Sequence 1. Fig. 7(a) shows the precharging waveform under an input voltage of 150 V. In the initial stage of Sequence 1, the transformer current is clamped to the maximum current of 50 A when the primary-side duty ratio D_1 is lower than 0.5. The duty ratio is limited by (6) or (7), which makes the operation effectively open-loop. As a result, the boost inductor current charges the capacitor in an unloaded LC circuit, which leads to LC resonance. The resonance current is damped over time because the parasitic resistances of the transformer and the inductor, and the forward voltage of the body-diode and the IGBT are considered in the simulation.

In Sequence 1, the charging of C_{dc}, C_{fc}, and C_{out} progresses. The duty command of D_1 is replaced with the PI controller output based on Fig. 2 when D_1 exceeds 0.5. A limit is applied to the current command in order to prevent saturation of the boost inductor. The limit value is defined by (9) as a variable, which clamps the peak current of the boost inductor to the design maximum value. During Sequence 1, V_{fcc} and V_{fcd} reach 750 V, which turns off Q_8 and Q_{12} and completes the charging of the flying capacitors. The sequence transitions from Sequence 1 to Sequence 2 when V_{dc} reaches the command value of 800 V. In Sequence 2, V_{out} is boosted to

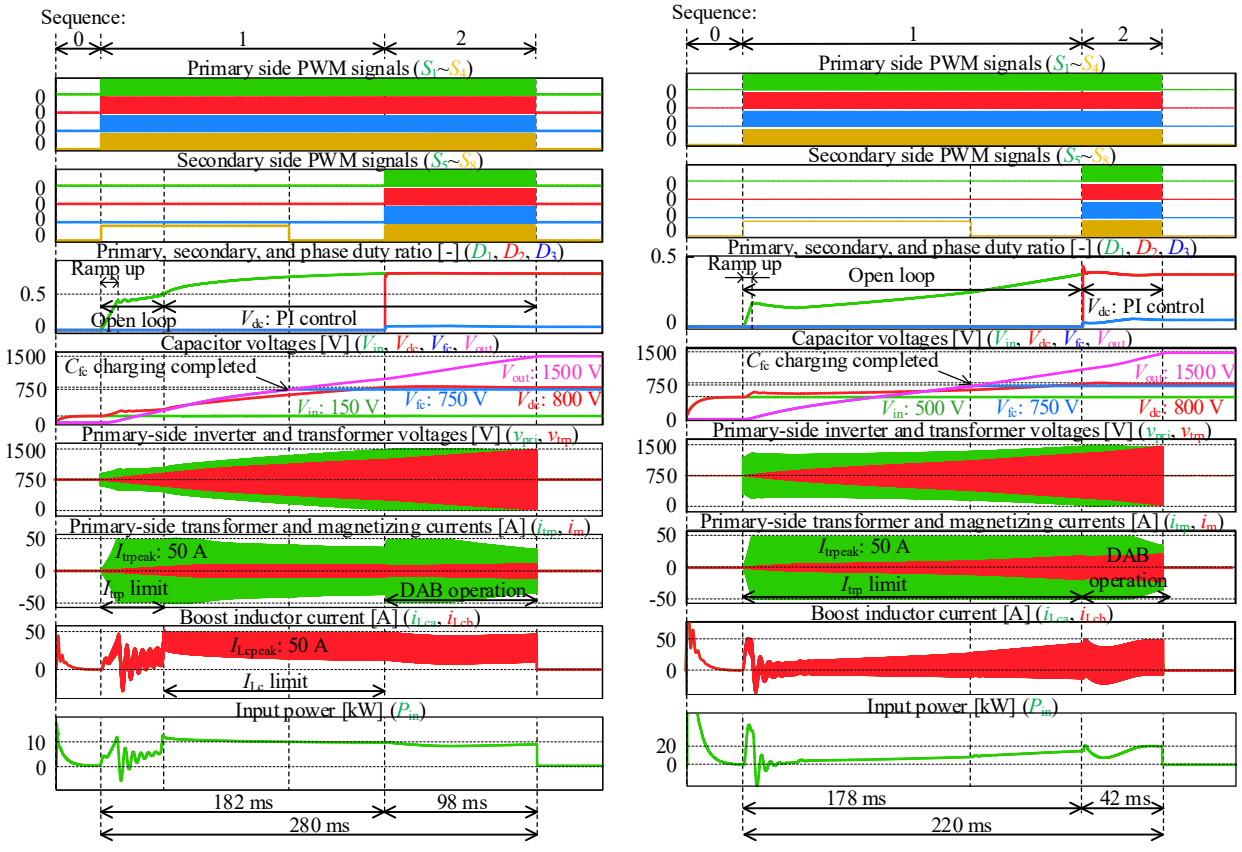

(a) V_{in} = 150 V (b) V_{in} = 500 V.

Fig. 7 Simulation waveforms of the precharging process. During the precharging operation, the transformer current or the boost inductor current is controlled to be clamped at the specified value. Thus, high-speed precharging is achieved.

1500 V. DAB operation is achieved by switching both the primary side and the secondary side in order to transfer power from the primary side to the secondary side. This operation enables charging to the desired output voltage regardless of the primary-side voltage. The phase shift D_3 between the primary side and the secondary side is controlled to keep the transformer peak current below the maximum value of 50 A.

Fig. 7(b) shows the simulation waveform under an input voltage of 500 V. The precharging process starts with a ramp increase of the primary-side duty ratio D_1, and the transformer current is clamped to the maximum current of 50 A, similar to Fig. 7(a). Under the condition of an input voltage of 500 V, the precharging process is completed while the primary-side duty ratio of D1 remains below 0.5. As a result, the transformer current is the only constraint during the precharging process under this condition.

V. Experimental Verifications

Fig. 8 shows the precharging waveforms under input voltages of 150 V and 500 V. In Fig. 8(a), current ringing appears at the beginning of switching, similar to Fig. 7(a). The boost inductor current is clamped to the specified peak value of 50 A by the PI control. The FCCF-DAB converter starts switching of both the primary side and the secondary side after the DC-bus voltage V_{dc} reaches 800 V. The FCCF-DAB converter then operates in DAB mode of the Sequence 2. Finally, the output voltage V_{out} increases and reaches 1500 V, which completes the precharging process.

In Fig. 8(b), the transformer current is clamped to the specified peak value of 50 A during the entire operation, which differs from Fig. 8(a). Ringing appears in the boost inductor current at the initial stage of charging and in the latter stage of sequence 1. This phenomenon is caused by the increased variation of the primary-side duty ratio D_1, which enhances the resonance. Under this test condition, the peak current does not significantly exceed 50 A. A limitation on the variation of D_1 is required for parameter sets that produce excessive current.

The error in the precharging time between the simulation and experimental results is 12 % at an input voltage of 150 V and 5% at an input voltage of 500 V. This mismatch is attributed to parameter variations of passive components. One factor is the capacitance tolerance of the capacitors used for charging. The electrolytic capacitors used in this study typically have a tolerance of 5% to 20%. In addition, (9), (13), and (16) are calculated based on the inductance values measured in advance, including the external inductance and leakage inductance L_{dab}, the magnetizing inductance L_m, and the boost inductance L_c. Thus, measurement errors and inductance variations under high current conditions of approximately 50 A introduce parameter deviations, which result in a slight difference in the precharging time between the simulation and experimental results. Although the charging current slightly exceeds the command value of 50 A due to inductance variations, the deviation is within approximately 5%, which indicates satisfactory performance.

In Mode I, during the initial stage of precharging, the transformer current is maintained at 50 A because the influence of the magnetizing current is small. The transformer peak current decreases in the latter stage of Sequence 1. A parameter error in the measured magnetizing inductance is considered in Mode II because the influence of the magnetizing current becomes significant.

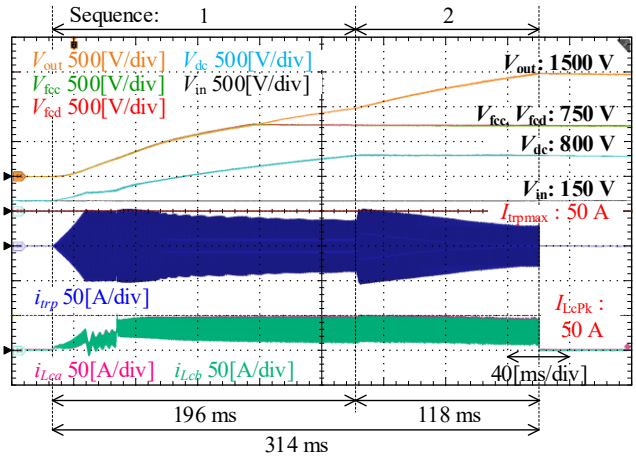

(a) Precharging waveform at V_{in} = 150 V

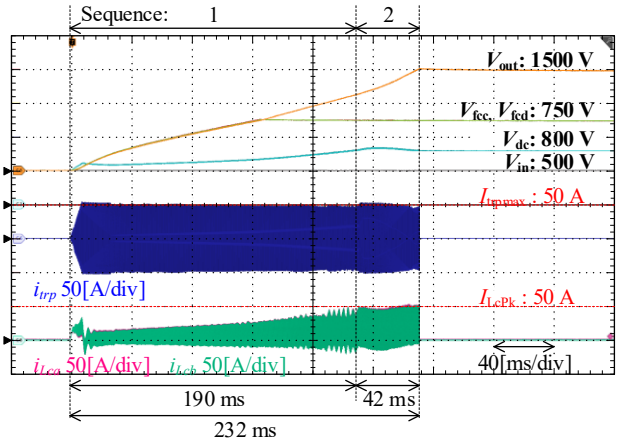

(b) Precharging waveform at V_{in} = 500 V.

Fig. 8 Experimental waveforms of the precharging process.

Fig. 9 shows the experimental waveforms of mode I and mode II under an input voltage of 150 V. The waveform of mode I appears immediately after the start of the precharging process. The operating mode transitions to mode II after the precharging process progresses to a certain level. In mode I of Fig. 9, the transformer current is properly controlled and maintained at the specified value of 50 A. In mode II, the peak value of the transformer current becomes lower than 50 A due to the limitation of the boost inductor current. The peak value of the boost inductor current is controlled at 50 A.

Fig. 10 shows the waveforms during the transition from Sequence 1 to Sequence 2. In Sequence 1, the secondary-side switches are turned off, and the converter operates in diode conduction mode. In Sequence 2, the secondary-side switches are turned on, and the converter operates in DAB mode. Fig. 10 shows the transition of the operating modes, which confirms that a seamless mode transition is achieved. No magnetic bias of the transformer current is observed during the mode transition.

VI. Conclusion

This paper presented an auxiliary-less precharging strategy for the flying-capacitor current-fed DAB converter and demonstrated its practical effectiveness through simulation and experimental verification. The proposed precharging method enables all capacitors, including the DC-

bus capacitor, the flying capacitors, and the output capacitor, to be charged to their target voltages without relying on any additional components. Throughout the entire precharging sequence, the transformer and boost-inductor currents are maintained within their designed saturation limits, ensuring safe and stable operation. The precharging time is consistent with the simulation results, with error of 12% at an input voltage of 150 V and 5% at 500 V. These results indicate that the precharging process is achieved under conditions comparable to those in the simulation. During limited to the designed value of 50 A, as verified experimentally. Thus, the effectiveness of the proposed precharging strategy is confirmed.

These results confirm that the proposed method provides a fast, simple, and reliable precharging solution suitable for practical implementation.

ACKNOWLEDGMENT

This work was supported by JST SPRING, Japan Grant Number JPMJSP2189.

REFERENCES

[1] S. Chen, G. Zhang, S. S. Yu, Y. Mei and Y. Zhang, "A Review of Isolated Bidirectional DC-DC Converters for Data Centers," *Chinese Journal of Electrical Engineering*, vol. 9, no. 4, pp. 1-22, December 2023.

[2] Y. Chen, K. Shi, M. Chen and D. Xu, "Data Center Power Supply Systems: From Grid Edge to Point-of-Load," *IEEE Journal of Emerging and Selected Topics in Power Electronics*, vol. 11, no. 3, pp. 2441-2456, June 2023.

[3] Sy Ngo, Thanh-Dong Ngo, "Improved MPPT Algorithm for Green Bus Stations using Solar Energy Systems," *IEEJ Journal of Industry Applications*, vol 14, issue 3, pp. 450-457, May, 2025.

[4] N. Yoshida, A. Kikuchi, T. Shimada, K. Ide, "Autonomous Decentralized DC Bus Voltage Control using DC Multi Power Units in DC Microgrid Applications," *IEEJ Journal of Industry Applications*, vol 13, no. 1, pp. 121-126, Nov. 2023.

[5] B. Stevanović, D. Serrano, M. Vasić, P. Alou, J. A. Oliver and J. A. Cobos, "Highly Efficient, Full ZVS, Hybrid, Multilevel DC/DC Topology for Two-Stage Grid-Connected 1500-V PV System With Employed 900-V SiC Devices," *IEEE Journal of Emerging and Selected Topics in Power Electronics*, vol. 7, no. 2, pp. 811-832, June 2019.

[6] T. Yasuda, J. Itoh, G. Guidi, S. D'Arco, "Intra-arm Balancing Control for Modular Multilevel Converter with Cell Loading Operated under High Power Imbalances," *IEEJ Journal of Industry Applications*, vol. 13, issue 3, pp. 317-326, May 2024.

[7] R. Kusui, K. Kusaka, H. Watanabe, J. Itoh, "Wireless Power Transfer System with Flying Capacitor Converters for Radiated Emission Harmonic Reduction," *IEEJ Journal of Industry Applications*, vol. 14, issue 2, pp. 232-239, March 2025.

[8] D. P. Nguyen, Y. Liu, X. Chen, H. Chiu, "GaN-Based Interleaved Four-level Flying Capacitor Triangular Conduction Mode (TCM) Converter with Coupled Inductors," *IEEJ Journal of Industry Applications*, vol. 13, issue 6, pp. 645-654, November 2024.

[9] D. P. Nguyen, Y. L., X. Chen, H. Chiu, "GaN-Based Interleaved Four-level Flying Capacitor Triangular Conduction Mode (TCM) Converter with Coupled Inductors," *IEEJ Journal of Industry Applications*, vol 13, no. 6, pp. 645-654, Nov. 2024.

[10] N. Fujii, and K. Hanamura, "ELECTRIC POWER CONVERSION DEVICE" International Patent WO 2019/111497 A1, Sep. 21, 2018.

[11] A. M. Y. M. Ghias, J. Pou, V. G. Agelidis and M. Ciobotaru, "Initial Capacitor Charging in Grid-Connected Flying Capacitor Multilevel Converters," *IEEE Transactions on Power Electronics*, vol. 29, no. 7, pp. 3245-3249, July 2014.

[12] S. Inoue and H. Akagi, "A Bidirectional DC–DC Converter for an Energy Storage System With Galvanic Isolation," *IEEE Transactions on Power Electronics*, vol. 22, no. 6, pp. 2299-2306, Nov. 2007.

[13] J. Hu, S. Cui and R. W. De Doncker, "Closed-Loop Black Start-Up of Dual-Active-Bridge Converter With Boosted Dynamics and Soft-Switching Operation," *IEEE Transactions on Power Electronics*, vol. 36, no. 10, pp. 11009-11013, Oct. 2021.

[14] J. Huang, Y. Wang, Z. Li and W. Lei, "Unified Triple-Phase-Shift Control to Minimize Current Stress and Achieve Full Soft-Switching of Isolated Bidirectional DC–DC Converter," *IEEE Transactions on Industrial Electronics*, vol. 63, no. 7, pp. 4169-4179, July 2016.

[15] T. Ohno, H. Watanabe and J. Itoh, "A Consideration about Loss Reduction by Boost Capacitor Voltage Control for Flying Capacitor-type Current-Fed DAB converter," IEEJ JIASC, no. 1-52, 2024.

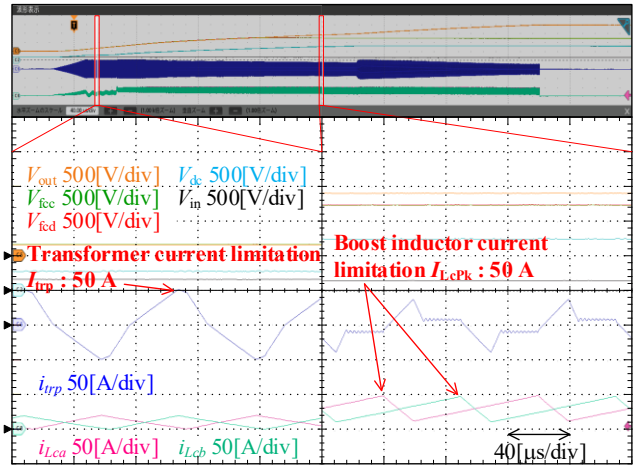

Fig. 9 Experimental waveform of Mode I and Mode II at V_{in} = 150 V. In Mode I, the peak transformer current is clamped at 50 A due to the transformer current limitation. In Mode II, the peak boost inductor current is clamped at 50 A due to the boost inductor current limitation.

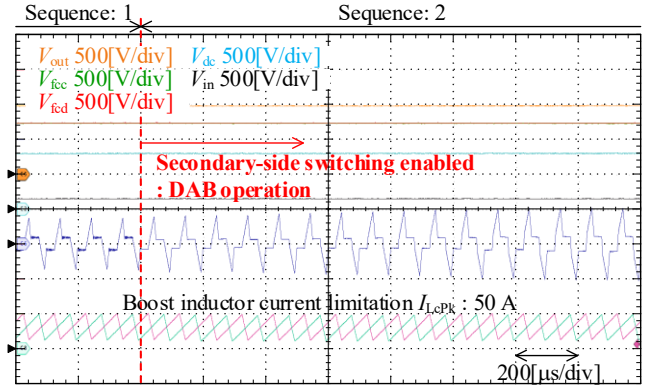

Fig. 10 Transition waveform from Sequence 1 to Sequence 2 at V_{in} = 150 V. The zoomed waveforms confirmed a seamless transition. DC bias is not observed in the transformer current.